Macromolecules
Article
Cite This: *Macromolecules* 2018, 51, 9890−9900
pubs.acs.org/Macromolecules

Tuning Arm Architecture Leads to Unusual Phase Behaviors in a $(BAB)_5$ Star Copolymer Melt

Lei Chen, Yicheng Qiang, and Weihua Li*

State Key Laboratory of Molecular Engineering of Polymers, Collaborative Innovation Center of Polymers and Polymer Composite Materials, Department of Macromolecular Science, Fudan University, Shanghai 200433, China

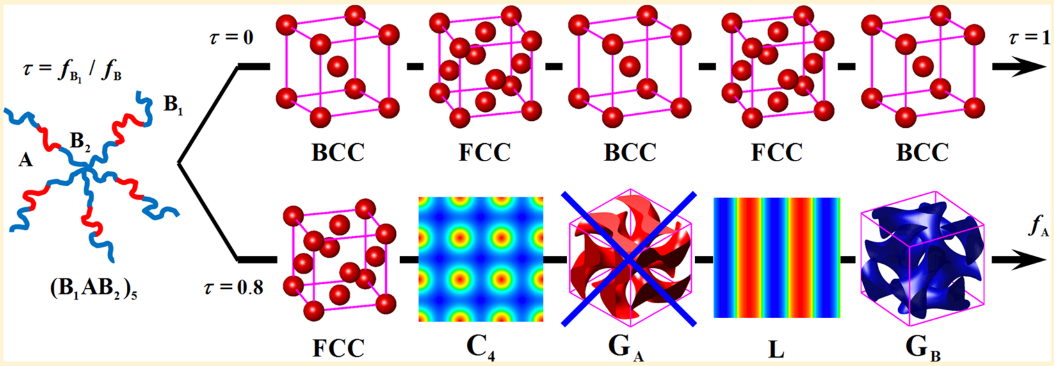

ABSTRACT: The self-assembly behavior of $(B_1AB_2)_5$ star copolymers, composed of five asymmetric BAB-triblock arms joined at the end of B_2-blocks, has been investigated using the self-consistent field theory. The special architecture enables a few different sophisticated mechanisms such as the conformational asymmetry from the star topology, the effect of combinatorial entropy from the multiple arms that enhances the formation of bridging configurations for the core B_2-blocks, the local segregation between the two different B-blocks, and the solubilization effect of the short B_2-block in the majority A-domain, each of which has been individually demonstrated to play an important role in impacting the self-assembly behavior of block copolymers before. As a result, the combination of these mechanisms leads to many unusual phase behaviors of $(B_1AB_2)_5$ with tunable asymmetry $\tau = f_{B_1}/(f_{B_1} + f_{B_2})$ between the two B-blocks, where f_{B_1} and f_{B_2} are the volume fractions of B_1- and B_2-blocks, respectively. For example, reentrant phase transitions between the BCC and FCC spherical phases are observed with minority A-domains, whereas the width of the overall spherical phase region at the opposite side of the phase diagram exhibits two maxima as τ increases. The expansion of the spherical phase region at the first maximum is induced by the reduced effective volume fraction due to the solubilization effect and thus is solely occupied by the BCC phase. While the expansion at the second maximum originates from the formation of enlarged "core−shell" domains due to the effect of local segregation, leading to the formation of complex Frank−Kasper spherical phases. In addition, no stable gyroid phase composed of A-network is observed in the phase diagram of $\tau = 4/5$, while the gyroid phase region in the opposite side of the phase diagram is expanded significantly. The absence of the gyroid phase is a very rare phenomenon for block copolymers and here may result from the combined effect of different sophisticated mechanisms.

INTRODUCTION

Self-assembly provides an important strategy for the fabrication of advanced nanomaterials. Block copolymers as a typical class of soft self-assembly systems have attracted intensive interest due to their remarkable advantages. First of all, block copolymers can self-assemble into rich ordered nanostructures with tunable nanoscale size of polymeric domains, which makes them exhibit a lot of potential applications.[1−9] Second, a number of advanced synthesis methods have been developed, which enables precise control of the molecular architectures of block copolymers and thus creates a huge space for novel ordered structures.[10] Third, the self-assembly behavior of block copolymers is predictable due to the well-established sophisticated theories, in particular, the self-consistent field theory (SCFT) as one of the most successful methods.[11−13] It has been demonstrated that SCFT is good at not only determining the stability of known ordered phases due to its unique ability of accurately calculating the free energy of each ordered structure but also exploring novel ordered phases coupled with appropriate initialization schemes.[14−19] Furthermore, SCFT can probe into the self-assembly mechanism of new structures by computing the different contributions of free energy as well as the distribution of each segment.[20−23] The fruitful interplay between experiment and theory rapidly advances the understanding on the self-assembly of block copolymers.[24−32]

Received: July 11, 2018
Revised: November 8, 2018
Published: November 29, 2018

DOI: 10.1021/acs.macromol.8b01484
Macromolecules 2018, 51, 9890−9900

Although the polymer architecture significantly impacts the self-assembly behavior of block copolymers, it does not often lead to the formation of novel ordered structures but only shifts the phase boundaries.[15,33] For example, the AB diblock copolymers form a number of ordered phases, including hexagonal close-packed (HCP) and body-centered-cubic (BCC) spheres,[15] hexagonal cylinders (C),[34] double gyroidal (G),[35] and *Fddd* (O^{70})[14] networks, and lamellae (L).[15,34] SCFT calculations have revealed that some more complex AB-type block copolymers, such as ABA triblock,[20,36−38] ABAB... multiblock,[19,39−44] and $(AB)_n$ star,[15,45−48] resemble the similar phase sequence as the AB diblock but with shifted phase boundaries. This observation implies that it would be infeasible to simply search the vast library of chain architectures for the fabrication of new ordered structures, and instead useful guiding principles are desired for the inverse design of block copolymer architectures.[10,16]

Usually a valid guiding principle could be derived from the well-established self-assembly mechanisms of some known block copolymers.[17] Although the self-assembly of block copolymers is governed by a simple general mechanism, i.e., the competition between the interfacial and entropic contributions to the free energy,[49] some sophisticated mechanisms are associated with the formation of a specific ordered phase, especially for some unconventional phases.[17] In contrast to the forward problem, i.e., exploring the phase behavior of a given block copolymer, to design block copolymers for targeting ordered structures as a typical inverse problem is more difficult to be solved due to the feature of multiple solutions.[50] In practice, it is more feasible to speculate a trial solution abiding by the derived guiding principles and then to verify the solution by exploring the stability region of the targeting ordered phase in the interesting parameter space of the considered block copolymer system. Importantly, more interesting phase behaviors beyond the formation of the targeting phase are often observed from the newly designed block copolymers.[16,17,30]

In recent years, a number of examples have been demonstrated with the inverse design of block copolymer systems, leading to the formation of some unconventional ordered phases including a large number of binary mesocrystals from linear BABCB multiblock copolymers,[16,51] complex Frank−Kasper spherical packing phases from conformation-asymmetric AB-type block copolymers[21] as well as binary blends of conformation-symmetric AB/AB diblock copolymers,[52] and square-array cylindrical phase (C_4) from $(BAB)_5$ multiarm star copolymers.[17] Among these designed block copolymers, the $(B_1AB_2)_m$ star copolymer, composed of m asymmetric B_1AB_2 triblock arms joined at the end of B_2-block, is of great interest. Actually, star architecture as one of the most fascinating ones consisting of unlike or identical arms has been made full use to design various interesting block copolymers that exhibit unique properties.[15,21,47,48,53−56] For example, the ABC miktoarm star copolymers self-assemble into many two-dimensional archimedean polygon-tiling patterns.[57−59] In particular, the multiple arms tend to be partitioned into as many as possible neighboring A-domains for maximizing the configurations, which is termed the effect of combinatorial entropy.[17,22,47,60] As a consequence, the joined B_2-blocks form effective bridges connecting neighboring A-domains. Moreover, the length of bridging blocks can be readily tuned by changing the relative length of B_2-block to the overall length of B-blocks, leading to the adjustable bridge blocks. It has been demonstrated that adjustable bridge block as a useful sophisticated mechanism is capable to regulate the coordination of crystalline phases, i.e., that the coordination numbers (CNs) of crystalline lattices tend to be lowered by shortening the bridge block.[16] As a result, the square-array cylindrical phase and the FCC spherical phase are predicted to be stable over the hexagonal phase (C_6) and the BCC phase with the $(B_1AB_2)_m$ star copolymers, respectively.[17]

Obviously, $(B_1AB_2)_m$ star copolymer with $\tau = N_{B_1}/(N_{B_1} + N_{B_2})$ can be reduced to the star copolymers of AB and BA diblock with $\tau = 0$ and 1, respectively. Note that the $(AB)_m/(BA)_m$ star copolymers are conformation-asymmetric, which indicates that the conformational asymmetry is continuously changed as τ and is reversed. It has been established that the conformational asymmetry as another important factor could lead to the formation of complex spherical packing phases.[21,25,45,54,61−63] An interesting question is whether unconventional spherical phase can be formed in $(B_1AB_2)_m$ star copolymers. In addition, we can speculate that two more sophisticated mechanisms might be realized in this special architecture, i.e., the solubilization effect of the short A-blocks in the majority B-domain that has been observed in asymmetric ABA triblock copolymers[36,38,64] and the local segregation between the two kinds of B-blocks that has been demonstrated in various AB-type multiblock copolymers.[15,55] The combination of these different sophisticated mechanisms may lead to many interesting phase behaviors. Recently, we noticed a pioneering SCFT work on the self-assembly of $(ABA')_3$ star copolymer by Fredrickson's group,[55] where some interesting phase behaviors have been predicted. In particular, they found that the asymmetry between the two A-blocks of the triblock arm influences the self-assembly behavior significantly. It is necessary to note that we considered the $(B_1AB_2)_5$ star copolymer with a larger number of arms aiming to enlarge the effect of combinatorial entropy of the multiple arms and thus to enhance the formation of bridging configurations for the core B_2-blocks. Fortunately, we predicted stable square-array cylinders and FCC spheres.[17] However, we mainly focused on the region of cylinders and spheres in the previous work. Therefore, it is necessary to re-examine the self-assembly of $(B_1AB_2)_5$ star copolymers to obtain more complete understanding on their phase behavior.

The self-consistent field theory (SCFT) has been proven as one of the most powerful methods for the exploration of phase behaviors of inhomogeneous polymeric systems.[11−13] In particular, for relatively flexible polymers that can be modeled by the Gaussian chain, efficient numerical methods have been developed to solve SCFT equations with reliable accuracy. Thus, SCFT has become a standard tool for the study of block copolymers like some experimental techniques (e.g., SAXS and TEM), especially for the formation of ordered phases far below the order−disorder transition (ODT) temperature where the thermal fluctuations can be ignored safely by the mean-field treatment. Accordingly, we will investigate the phase behavior of $(B_1AB_2)_5$ star copolymers using SCFT. Here we choose the pseudospectral method[65−67] to solve SCFT equations, which is not only highly efficient because of the advantage of the fast Fourier transform and the use of the accelerating Anderson mixing scheme[68] to speed up the converging process but also powerful to deal with distinct complex ordered phases when coupled with the special initialization scheme.[16,18]

DOI: 10.1021/acs.macromol.8b01484
Macromolecules 2018, 51, 9890−9900

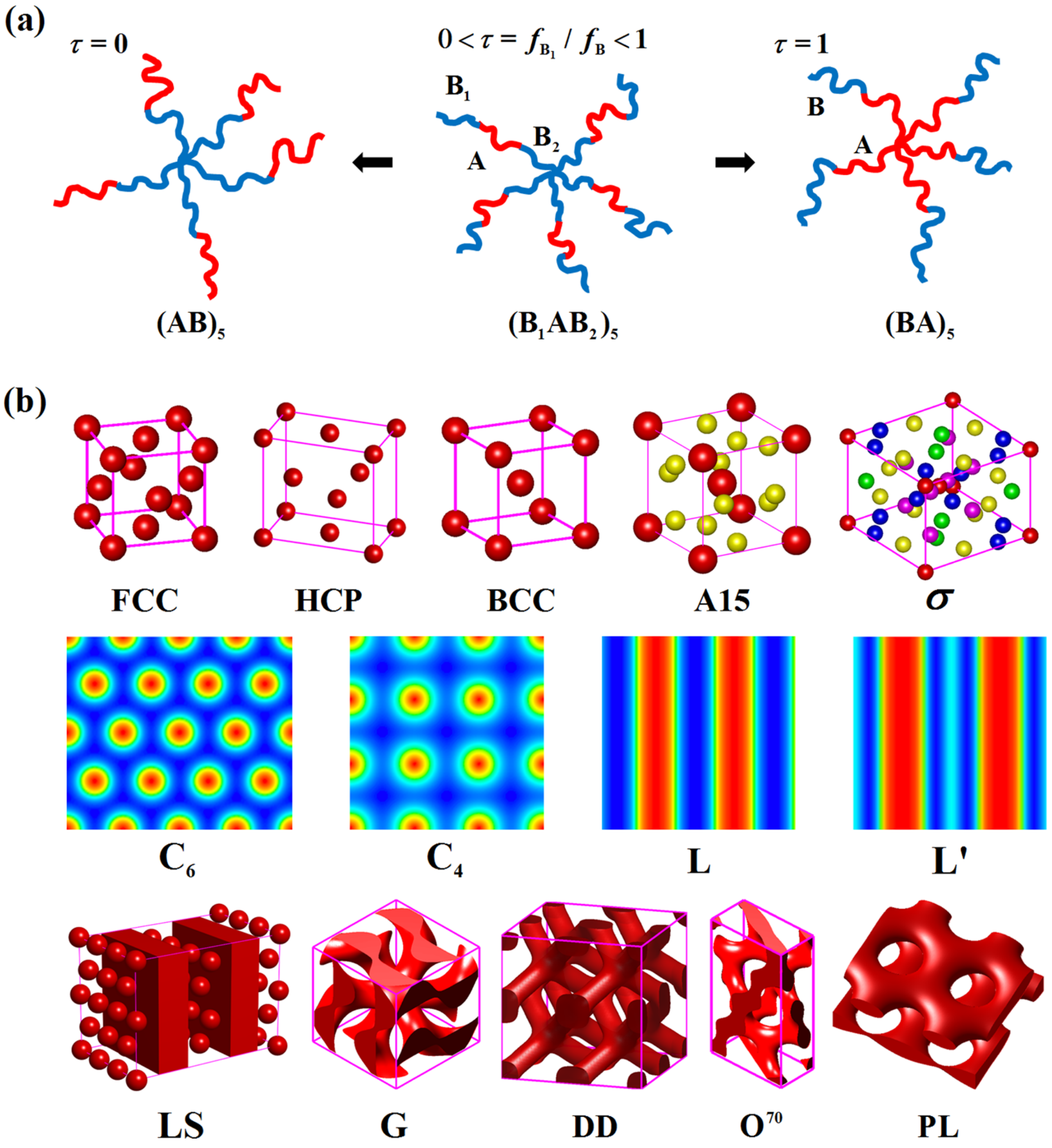

Figure 1. (a) Center: schematic of $(B_1AB_2)_5$-triblock star copolymer with the arms joined at the end of B_2-blocks. The asymmetry of length between the two B-blocks is characterized by $\tau = f_{B_1}/f_B$. The star copolymer is reduced to $(AB)_5$ with $\tau = 0$ in the left panel while it becomes $(BA)_5$ with $\tau = 1$ in the right panel. (b) Schematics of the candidate ordered phases considered in this work, including five different spherical phases (FCC, HCP, BCC, A15, and σ), hexagonal (C_6) and square (C_4) cylindrical phases, regular lamellar (L) and sandwich-like lamellar (L′) phases, hybrid lamella−sphere (LS) phase, and four continuous phases [double gyroid (G), double diamond (D), *Fddd* network (O^{70}), and perforated lamellae (PL)].

■ THEORY AND METHOD

We consider a melt consisting of n identical $(B_1AB_2)_m$ star copolymer chains in a volume of V, each of which is composed of m B_1AB_2-triblock arms joined at the end of B_2-block. The total number of segments of each B_1AB_2 arm is N, and the volume fractions of A- and B-blocks are denoted as $f_A = f$ and f_B ($f_A + f_B = 1$). The A-/B-segments are assumed to have equal density ρ_0 and segment length b. Thus, the segment numbers of each B_1-, A-, and B_2-block are specified as $f_{B_1}N$, f_AN, and $f_{B_2}N$, respectively, with $f_{B_1} + f_{B_2} = f_B$. An additional variable, $\tau = f_{B_1}/f_B$, is introduced to characterize the asymmetry of length between the two B-blocks. Apparently, the copolymer is reduced to $(AB)_m$ and $(BA)_m$ star copolymers when $\tau = 0$ and 1, respectively (Figure 1).

For this copolymer melt under the assumption of incompressibility condition, the free energy functional at temperature T in the framework of SCFT can be expressed as[13]

$$\frac{F}{nk_BT} = -\ln Q + \frac{m}{V}\int d\mathbf{r}\{\chi N\phi_A(\mathbf{r})\phi_B(\mathbf{r}) - w_A(\mathbf{r})\phi_A(\mathbf{r}) - w_B(\mathbf{r})\phi_B(\mathbf{r}) - \eta(\mathbf{r})[1 - \phi_A(\mathbf{r}) - \phi_B(\mathbf{r})]\} \quad (1)$$

where $V = nmN/\rho_0$ and k_B is the Boltzmann constant. In eq 1, $\phi_A(\mathbf{r})$ and $\phi_B(\mathbf{r})$ are the volume fraction distributions of A- and B-segments, while $w_A(\mathbf{r})$ and $w_B(\mathbf{r})$ are their conjugate mean fields, respectively. The spatial function $\eta(\mathbf{r})$ is the Lagrange multiplier used to enforcing the incompressibility condition, $\phi_A(\mathbf{r}) + \phi_B(\mathbf{r}) = 1$. The constant quantity Q is the partition function of single chain interacting with the mean

DOI: 10.1021/acs.macromol.8b01484
Macromolecules 2018, 51, 9890−9900

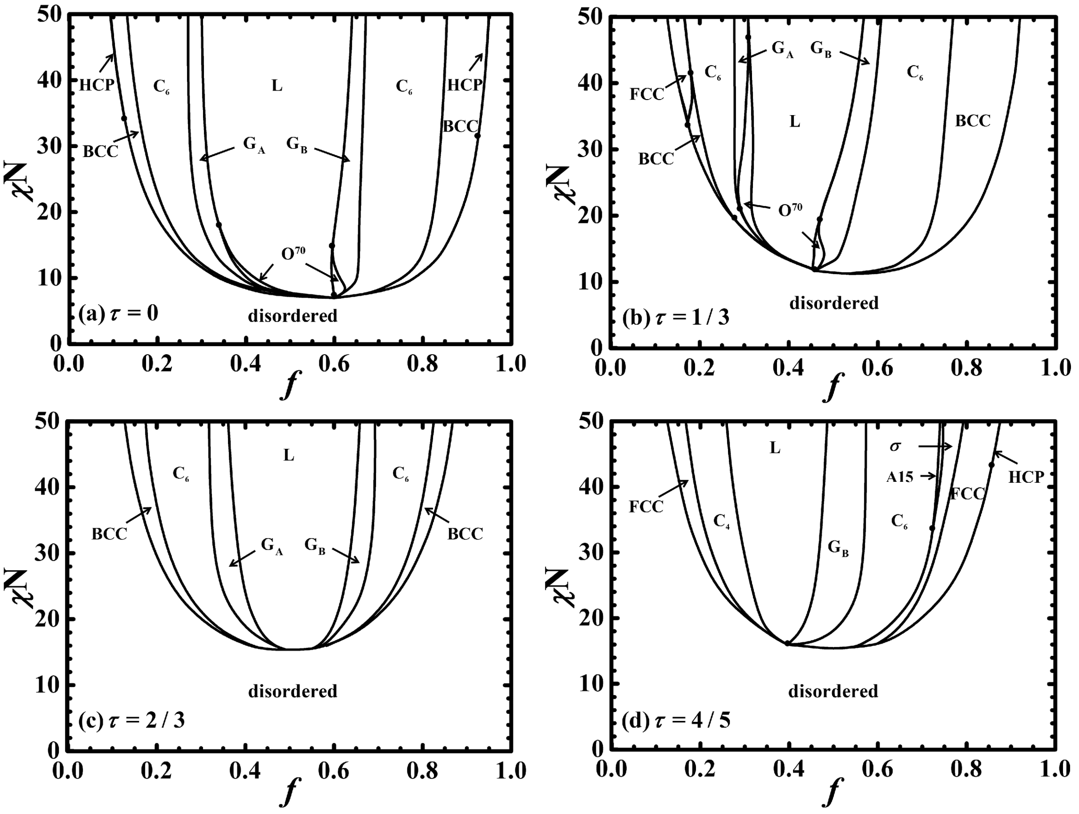

Figure 2. Phase diagrams at the f–χN plane of $(B_1AB_2)_5$ star copolymers with various values of τ: (a) $\tau = 0$ (i.e., $(AB)_5$); (b) $\tau = 1/3$; (c) $\tau = 2/3$; (d) $\tau = 4/5$.

fields $w_A(\mathbf{r})$ and $w_B(\mathbf{r})$. The SCFT equations associated with the free energy functional in eq 1 are written as

$$w_A(\mathbf{r}) = \chi N\phi_B(\mathbf{r}) + \eta(\mathbf{r}) \tag{2}$$

$$w_B(\mathbf{r}) = \chi N\phi_A(\mathbf{r}) + \eta(\mathbf{r}) \tag{3}$$

$$\phi_A(\mathbf{r}) = \frac{1}{Q}\int_{s\in A} \mathrm{d}s\, q(\mathbf{r}, s)q^{\dagger}(\mathbf{r}, s) \tag{4}$$

$$\phi_B(\mathbf{r}) = \frac{1}{Q}\int_{s\in B} \mathrm{d}s\, q(\mathbf{r}, s)q^{\dagger}(\mathbf{r}, s) \tag{5}$$

$$Q = \frac{1}{V}\int \mathrm{d}\mathbf{r}\, q(\mathbf{r}, s)q^{\dagger}(\mathbf{r}, s) \tag{6}$$

Here $q(\mathbf{r},s)$ and $q^{\dagger}(\mathbf{r},s)$ are the propagators of the polymer chain, satisfying the following modified diffusion equations

$$\frac{\partial q(\mathbf{r}, s)}{\partial s} = \nabla^2 q(\mathbf{r}, s) - w(\mathbf{r}, s)q(\mathbf{r}, s) \tag{7}$$

$$-\frac{\partial q^{\dagger}(\mathbf{r}, s)}{\partial s} = \nabla^2 q^{\dagger}(\mathbf{r}, s) - w(\mathbf{r}, s)q^{\dagger}(\mathbf{r}, s) \tag{8}$$

where $w(\mathbf{r},s) = w_K(\mathbf{r})$ when s belongs to the K-block (K = A and B). The initial conditions are $q(\mathbf{r},0) = 1$ at the free ends, while $q^{\dagger}(\mathbf{r},1) = [q(\mathbf{r},1)]^{m-1}$ at the junction point. In the above expressions, the radius of gyration of a unperturbed homopolymer chain with N segments, $R_g = N^{1/2}b/\sqrt{6}$, is chosen as the unit of spatial length. More detailed information about SCFT can be found in the literature.[12,13] Moreover, a standard discretization scheme[23] of the pseudospectral method[67] is used in this work to ensure a reliable accuracy with the calculation of phase boundaries.[65,66]

■ RESULTS AND DISCUSSION

Apparently, the self-assembly behavior of $(B_1AB_2)_5$ star copolymers is controlled by three parameters: χN, f, and τ. In our previous work,[17] the phase diagram with respect to f and τ for a fixed χN has been investigated, where noticeable stability regions of the C_4 and FCC phases are identified. In experiments, the value of χN can be readily tuned by varying the polymerization degree of the polymer or the temperature because of the usual relationship of $\chi \sim 1/T$.[1] So we will first construct a series of phase diagrams at the f–χN plane for a few typical values of τ.

To make the phase diagram as reliable as possible, we have considered a few unconventional ordered phases besides those conventional ones (HCP, FCC, BCC, C_6, G, O^{70}, and L), including Frank–Kasper σ and A15 spherical phases, square-array cylindrical phase (C_4), sandwich-like lamellar phase (L′), hybrid lamella–sphere phase (LS),[19] double diamond phase (D), and perforated lamellar phase (PL) (Figure 1). Note that there are two different morphologies of the PL phase differing in the arrangement of holes in the neighboring perforated layers, i.e., abab... and abcabc... sequences.[69,70] Matsen has predicted using the highly accurate spectral method of SCFT that the two kinds of PL morphologies has very tiny free energy difference.[70] So here we just consider one of the PL morphologies with the abab... arrangement of the holes. Similarly, there are abab... and abcabc... layering sequences of spheres for the LS morphology, and thus we also just consider the former one in our SCFT calculations. A cubic/rectangular structural unit for each ordered three-/two-dimensional

DOI: 10.1021/acs.macromol.8b01484
Macromolecules 2018, 51, 9890−9900

morphology is chosen to calculate the free energy. The free energy is minimized with respect to the sizes of the cubic/rectangular box that is put onto a grid lattice for discretization by a special initialization. To obtain reliable accuracy with the phase transition points, we choose the grid lattice as 128 × 128 × 64 for the complex Frank−Kasper σ phase and 64^3 for the other three-dimensional phases, while 64^2 for the lamellar and cylindrical phases. Such large grid lattices ensure the grid spacing smaller than $0.1R_g$. The chain contour is divided with a step size of Δs = 0.002−0.005. Moreover, a stringent convergence criteria is employed for the solving iteration of the SCFT equations, i.e., that the free energy, the volume fractions (or mean fields), and the incompressibility condition converge to a computational error less than 10^{-8}.

The phase diagrams for τ = 0, 1/3, 2/3, and 4/5 are presented in Figure 2. Obviously, the four phase diagrams differ from each other dramatically, in particular, three of which with $0 < \tau < 1$ exhibit very different features. The phase diagram of $(AB)_5$ in Figure 2a is similar to that of $(AB)_9$ calculated using the spectral method by Matsen.[15] As expected, the star architecture breaks the conformational symmetry between A- and B-blocks, thus leading to the asymmetric phase diagram where the phase regions of B-cylinders and B-spheres are notably expanded in contrast to those with minority A-domains. However, it is necessary to pay attention to two features. The first feature is that the asymmetry of the phase diagram does not change significantly when the number of arms increases from 5 to 9. The other feature is that the asymmetry of the phase diagram of $(AB)_m$ is less pronounced than that of the miktoarm star copolymer of AB_m.[15,54] Specifically, the phase diagram of $(AB)_m$ is even less asymmetric than that of AB_2.[21] In other words, the conformational asymmetry induced by the star topology of $(AB)_m$ is smaller than that induced by the B-branching architecture of AB_m.[71] The main reason is that the unequal number of A and B blocks in AB_m leads to highly asymmetric stretching degrees between them, thus creating a large tendency of forming spontaneous curvature toward the A-domain. As a consequence, the overall spherical region with minority B-dimains in the phase diagram of $(AB)_5$ is not expanded large enough for the formation of complex Frank−Kasper spherical phases that are observed in the phase diagrams of AB_m.[21]

When τ is increased to 1/3, surprisingly the phase diagram in Figure 2b becomes more asymmetric than that of τ = 0. In contrast, the asymmetry of the phase diagram for τ = 2/3 in Figure 2c decreases, while that of τ = 4/5 in Figure 2d increases once again. This observation implies more sophisticated mechanisms besides the effect of conformational asymmetry. Moreover, the change of the phase diagrams as τ is accompanied by the presence of many unusual phase behaviors. Therefore, we will probe into these sophisticated mechanisms by examining each unusual phase behavior in these phase diagrams.

One of the remarkable phase behaviors lies in the stable phase of A-spheres in the phase diagrams, which changes from pure BCC in the phase diagram of τ = 0 to competing BCC/FCC in that of τ = 1/3 and pure BCC once again in that of τ = 2/3 and then to pure FCC in that of τ = 4/5. Of course, finally the stable spherical phase transfers from FCC back to BCC when τ increases from 4/5 to 1 because the $(BAB)_5$ star copolymer is reduced to $(BA)_5$ star copolymer at τ = 1, of which the phase region of A-spheres is the mirror image of that of B-spheres in the phase diagram of $(AB)_5$ in Figure 2a. In our previous work,[16,17] it has been demonstrated that the adjustable bridge blocks enabled by the effect of combinatorial entropy of the multiple arms play a critical role in impacting the transition between the crystalline phases of discrete domains. However, here the reentrant BCC/FCC transitions should not be induced by only one sophisticated mechanism.

To demonstrate the reentrant BCC/FCC transitions as τ increases, we plot their free energies as a function of τ in Figure 3. There are twice reentries into the FCC phase at $\tau \approx 0.17$ and 0.73, respectively, for the specific group of parameters χN = 50 and f = 0.15. In other words, the FCC phase exhibits two stability regions, which are $0.17 \lesssim \tau \lesssim 0.36$ and $0.73 \lesssim \tau \lesssim 0.84$, respectively. As a comparison, we also calculate the free energy of FCC relative to BCC formed in the linear B_1AB_2 triblock copolymers with the same length and composition as the triblock arm of the star copolymer for χN = 50. In great contrast, FCC is always less stable than BCC though their free energy difference exhibits double minima as τ increases for the

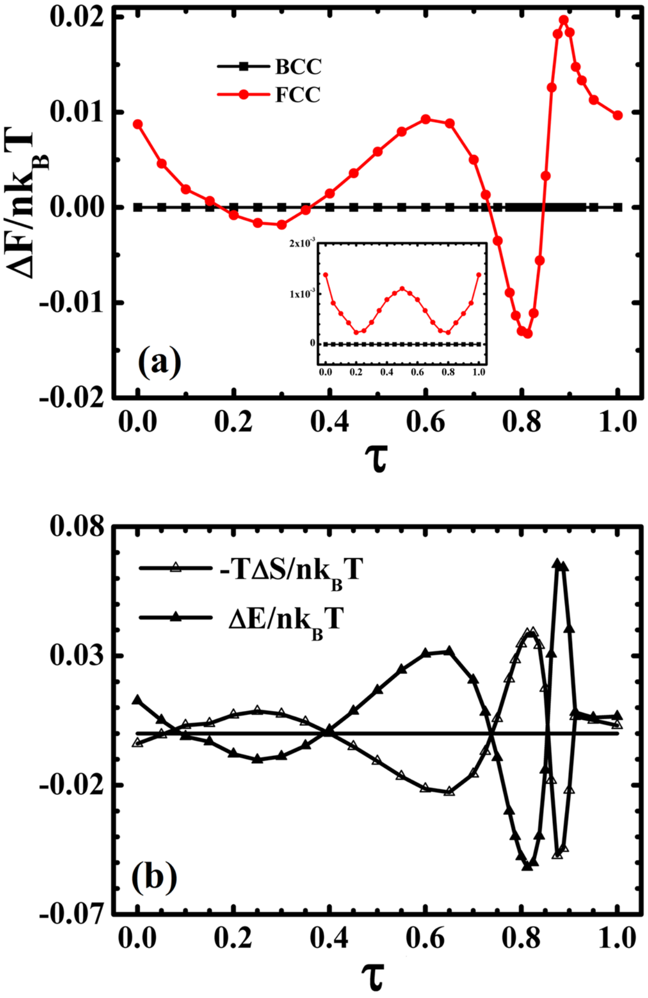

Figure 3. (a) Free energy of the FCC spherical phase relative to BCC as a function of τ for given χN = 50 and f = 0.15. The inset shows the free energy comparison between BCC and FCC self-assembled by the linear B_1AB_2 triblock copolymers with the same length and composition as the triblock arm of the star copolymer for χN = 50. (b) Interfacial (filled triangles) and entropic contributions (unfilled triangles) to the free energy of the FCC phase relative to BCC along the same phase path as that of (a).

asymmetric linear triblock copolymer. This observation indicates that the reentrant BCC/FCC transitions should be attributed to the star topology of $(B_1AB_2)_5$.

Matsen has proposed that the FCC (or HCP) phase is usually less stable than the BCC phase due to the higher packing frustration. Furthermore, he has argued that the FCC phase could become stable only when the packing frustration is relieved by some extra factors, such as a small population of solubilized diblocks into the matrix at the vicinity of the ODT boundary or polydispersity.[72] This suggests that the FCC phase in the current star copolymers may be also stabilized by the reduced packing frustration. As the packing frustration is closely related to the distribution of each segments, we will look for the evidence from the distribution of some characteristic segments.

As discussed before, one of the most important effects stemming from the star topology is the effect of combinatorial entropy, i.e., driving the multiple arms to be partitioned into as many discrete domains as possible.[17,22] As a consequence, the junction points are localized by the partition of these arms in response to the coordination environment of the spherical phases. Coupling with the rule of uniformly filling the space, the distribution of the junction points would have a severe impact on the distributions of segments, especially for the segments on the two different B-blocks in the $(B_1AB_2)_5$ star copolymer.

We start from the $(AB)_5$ star copolymer ($\tau = 0$) to illustrate the distribution of the junction points. On the basis of the simple geometrical analysis, we can determine the most probable locations (MPLs) of the junction points in the BCC morphology. There are four equivalent MPLs on each face of the structural unit (Figure 4a$_1$). Note that the MPL is furthest from the domain center. Specifically, a pair of the MPLs is on each central line of the square face and separated by $a^{\mathrm{BCC}}/4$ from the nearest edge, where a^{BCC} is the edge length of the cubic unit. The multiple arms of each star copolymer starting from each MPL can be partitioned at the most into four domains. Thus, the distance from each MPL to the domain center is $l^{\mathrm{BCC}} = \sqrt{5}/4a^{\mathrm{BCC}} \approx 0.56a^{\mathrm{BCC}}$. Here the distribution of the junction point is characterized by $\rho_{\mathrm{joint}}(\mathbf{r}) = q(\mathbf{r},0)q^{\dagger}(\mathbf{r},0)/Q$.[22] In Figures 4b$_1$ and 4b$_2$, the isosurfaces of $\rho_{\mathrm{joint}}(\mathbf{r})$ at ρ_{joint} = 7 and 7.5 are plotted for the BCC morphology formed by $(AB)_5$ with $f = 0.1$ and $\chi N = 50$.

In contrast to BCC, there are two kinds of possible MPLs in the FCC morphology, which are at the centers of a regular octahedron and a regular tetrahedron, respectively (Figure 4). The distances from the two MPLs to their respective domain center are $l_1^{\mathrm{FCC}} = 0.5a^{\mathrm{FCC}}$ and $l_2^{\mathrm{FCC}} = \sqrt{3}/4a^{\mathrm{FCC}} \approx 0.43a^{\mathrm{FCC}}$ with a^{FCC} the edge length of the FCC unit, respectively. Figures 4b$_3$ and 4b$_4$ demonstrate the distribution of the junction points in the FCC morphology, suggesting that the junction point has a higher probability at the center of the regular octahedron than at the center of the regular tetrahedron because of the larger number of domains accessed by the arms. Our SCFT calculations indicate that the spherical domains in the BCC and FCC morphologies for the same group of parameters have similar size, leading to $a_{\mathrm{FCC}} \approx 2^{1/3}a_{\mathrm{BCC}}$. Accordingly, we can get the relationship of $l_2^{\mathrm{FCC}} \approx 0.54a^{\mathrm{BCC}} < l^{\mathrm{BCC}} \approx 0.56a^{\mathrm{BCC}} < l_1^{\mathrm{FCC}} \approx 0.63a^{\mathrm{BCC}}$.

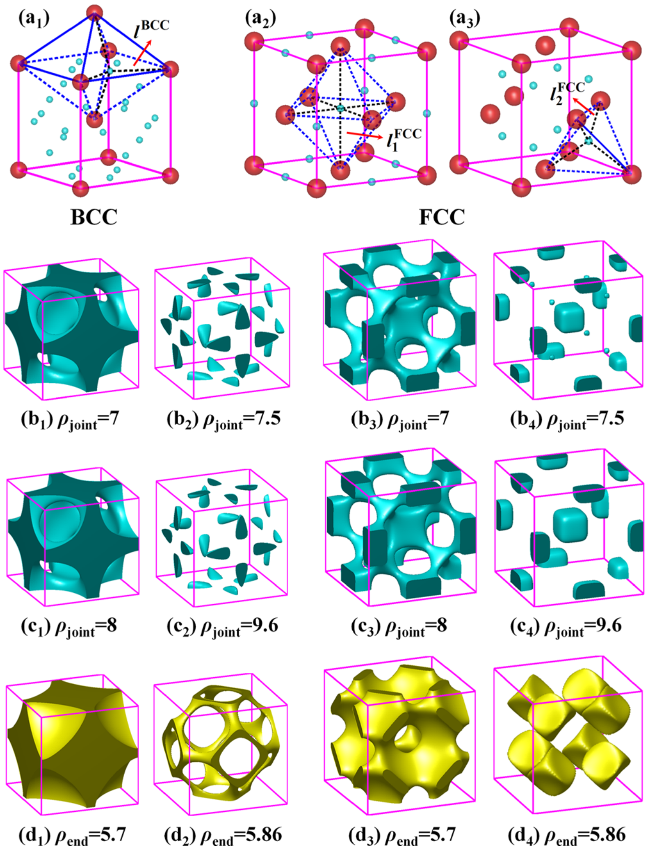

Figure 4. (a) Schematics showing the most probable locations (cyan dots) of the junction points of the $(AB)_5$ ($\tau = 0$) star copolymers in the BCC and FCC morphologies, where the minority A-domains are plotted as the red spheres. In BCC (a$_1$), each face of the structural unit has four most probable locations, each of which has an equal distance (l^{BCC}) indicated by the black dashed lines to the centers of four A-domains belonging to an octahedron drawn by the blue solid/dashed lines. While in FCC, there are two possible most probable locations, which are located in the centers of a regular octahedron (a$_2$) and a regular tetrahedron (a$_3$) drawn by the blue solid/dashed lines, respectively. The distances between the center and the vertices of the octahedron and the tetrahedron are denoted as l_1^{FCC} and l_2^{FCC}, respectively. (b$_1$−b$_4$) Isosurface plots of the distribution of the junction points in the BCC (b$_1$ and b$_2$) and FCC (b$_3$ and b$_4$) morphologies for $(AB)_5$ ($\tau = 0$) with $f = 0.1$ and $\chi N = 50$. (c$_1$−c$_4$) Distributions of the junction points in the BCC and FCC morphologies for $(B_1AB_2)_5$ with $\tau = 0.3$, $f = 0.15$, and $\chi N = 50$. (d$_1$−d$_4$) Distributions of the free B-ends in the BCC and FCC morphologies for the same systems in (c).

For $\tau = 0$, there is only one type of B-blocks to form the matrix. In the FCC morphology, the B-blocks extending from the two different kinds of MPLs to reach the respective A-domains experience unequal degrees of stretching, leading to an extra packing frustration compared with those in the BCC morphology. Therefore, FCC is usually less stable than BCC, which is similar to the case in the AB diblock copolymer melt. When the B-block is divided into B$_1$- and B$_2$-blocks by the A-block, the two B-blocks could fill different areas of the matrix in either BCC or FCC and thus could regulate the packing frustration. In general, as τ increases, increasing B$_1$-block extends to further space while shortening B$_2$-block moves away from the MPLs in Figure 4a. Here we introduce the distribution of the free B-ends, $\rho_{\mathrm{end}}(\mathbf{r}) = q(\mathbf{r},1)q^{\dagger}(\mathbf{r},1)/Q$, to characterize the distribution of B$_1$-blocks. Specifically, for $0.17 \lesssim \tau \lesssim 0.36$, the short B$_1$-block tends to stay around the spherical domains (Figure 4d), enforcing the junction points to be more enriched around the MPLs (Figure 4c). However, the coordinate environment of FCC favors the redistribution of the two B-blocks than that of BCC. The main reason lies in that the short B_1-blocks are enriched in the central region of the tetrahedra, expelling the junction points to the central region of the octahedra in the FCC morphology (Figure 4c,d). On one hand, the localization of the junction points in the central region of the octahedra benefits the combinatorial entropy. On the other hand, the local segregation of the two different B-blocks relieves the packing frustration in the FCC morphology. On the whole, the local segregation of the two kinds of B-blocks is unfavored by the entropic contribution to the free energy but benefits the interfacial energy (Figure 3b). When the gain of the interfacial energy could compensate the energy penalty of entropy, the FCC becomes stable over BCC.

When $\tau > 0.36$, the junction points are driven by the increasing stretching of the bridging B_2-blocks to leave the central region of the octahedra (e.g., $\tau = 0.6$ in Figure 5a,b). In other words, the B_1- and B_2-blocks cannot be favorably distributed to the tetrahedral and octahedral areas, respectively, in the FCC morphology. As a result, the extra packing frustration of the FCC phase is not effectively released, and its combinatorial entropy from the large accessible domain number (e.g., 6) of the multiple arms in the octahedral area is not fully maximized, making it become less stable than the BCC phase. For a large τ (e.g., $\tau = 0.8$ in Figure 5c,d) or short B_2-blocks, the junction points move to the bonding area between two neighboring domains to release the high stretching of the bridging B_2-blocks. In the range of $0.73 \lesssim \tau \lesssim 0.84$, the bridging B_2-blocks become extremely stretched, thus driving the crystalline lattice to transform from BCC to FCC of lower coordination number (CN). Note that the CN of FCC is given by the number of the 12 nearest-neighbor domains (NNDs) of every domain, i.e., CN = 12, while that of BCC depends on not only 8 NNDs but also the 6 next-nearest-neighbor domains (NNNDs). By rescaling the contribution of each NNND by the ratio of the squares of the NND distance to the NNND distance, i.e. $(\sqrt{3}/2)^2$, the effective CN of BCC is estimated, CN = 8 + 3/4 × 6 = 12.5.

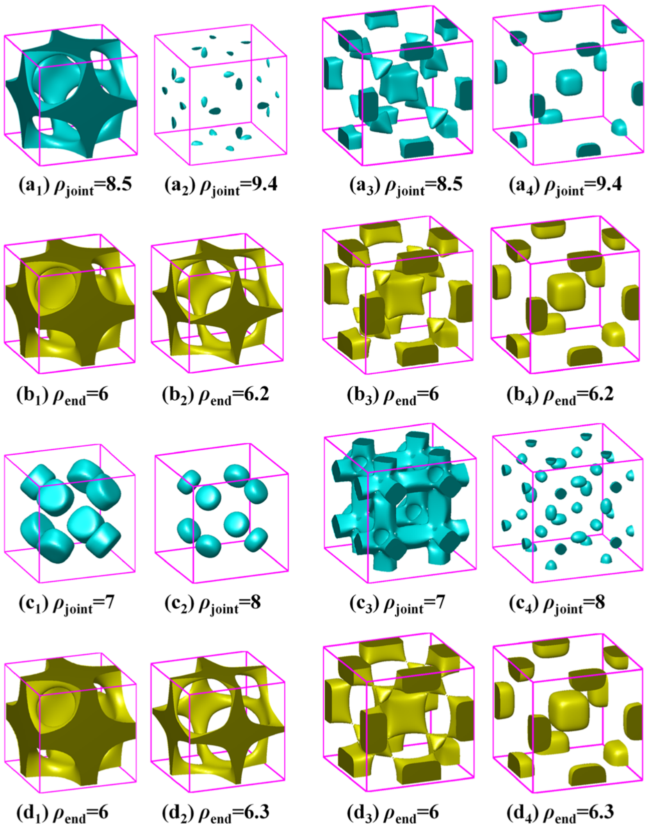

Figure 5. Distributions of the junction points and the free B-ends in the BCC and FCC morphologies for $(B_1AB_2)_5$ with $f = 0.15$ and χN = 50: (a, b) $\tau = 0.6$; (c, d) $\tau = 0.8$.

Figure 6 indicates that the bridging fraction for either BCC or FCC phase decreases as τ, and it decreases rapidly in the range of $0.73 < \tau < 0.84$. Although the bridging fractions of the two phases differ slightly, the difference becomes more pronounced in $0.73 < \tau < 0.84$. The higher bridging fraction of FCC than BCC makes the former phase more stable. It is necessary to note that the free energy difference induced by the effect of stretched bridge block is notably larger than that induced by the packing frustration release within $0.17 < \tau < 0.36$. Smaller domain spacing as well as larger domain size can be achieved in the crystalline phase of lower CN, benefiting postponing the disruption of the bridging configurations and at the same time favoring the interfacial energy.[17] As long as the bridging configurations of B_2-blocks are unavoidably disrupted for very short B_2-blocks such as $\tau > 0.84$, the FCC phase becomes less stable than BCC once again. In a word, the reentrant BCC/FCC transitions are dictated by the change of the chain configurations governed by the conventional chain packing rule and additional effect of combinatorial entropy from the multiple arms.

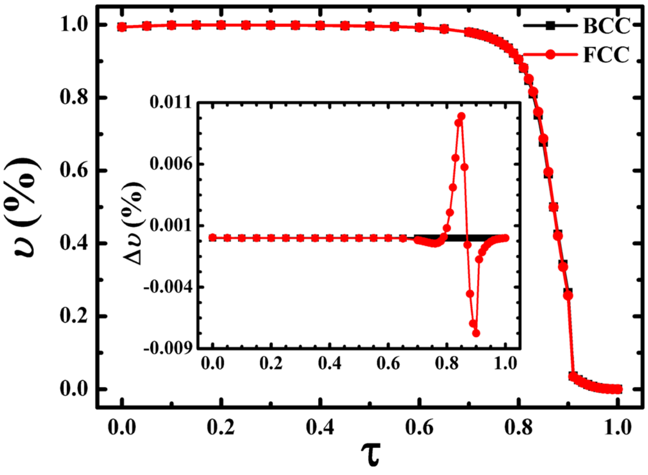

Figure 6. Comparison of the bridging fraction between the BCC and FCC phases for χN = 50 and $f = 0.15$. The inset shows the difference of the bridging fractions between the two spherical phases.

It is necessary to note that the highly asymmetric phase diagram of Figure 2b exhibits large regions of cylinder and sphere. More surprisingly, such large spherical phase region is solely occupied by the BCC phase (Figure 7). It is well-known that the expansion of spherical phase region is usually accompanied by the appearance of complex Frank−Kasper σ or A15 spherical phases. It is also known that the complex crystalline lattice of σ or A15 has rounder Wigner−Seitz cells[26] that benefit the packing of large domains with small deformation and thus favorable interfacial energy.[21,30] This argument implies that the spherical B-domain in the BCC phase region with a large volume fraction f_B should not be

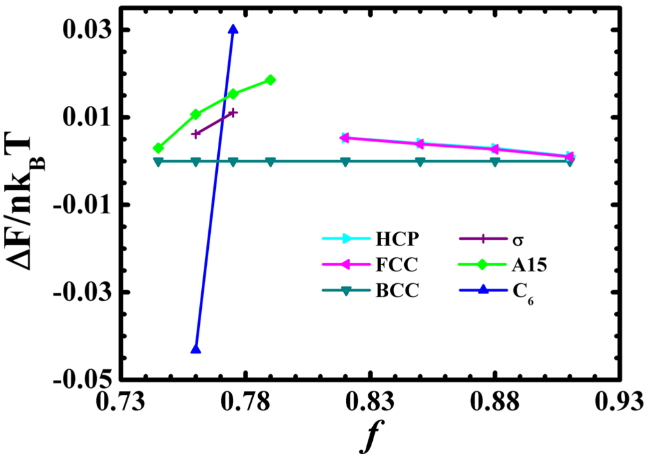

Figure 7. Free energies of considered ordered phases relative to that of the BCC phase for $(B_1AB_2)_5$ with $\tau = 1/3$ and $\chi N = 50$.

large. In other words, the volume fraction of B-domains, termed f_B^{eff}, is lower than the intrinsic volume fraction of B-blocks, f_B. To verify this speculation, we estimate the difference of $\Delta f_B = f_B - f_B^{eff}$ in Figure 8, indicating notable deviations of f_B^{eff} from f_B. Note that the effective volume fraction of f_B^{eff} is calculated with the A/B interfaces at $\phi_A(\mathbf{r}) = \phi_A(\mathbf{r}) = 0.5$. Such considerable deviation is induced by the partial solubilization of the short B_2-cores because of more gain in the configurational entropy but at the low cost of A/B_2 interfacial energy. The solubilization effect is observed previously in the self-assemblies of asymmetric ABA triblock[36] and ABAB tetrablock[19,44] copolymers, and it attenuates as f_{B_2} increases.

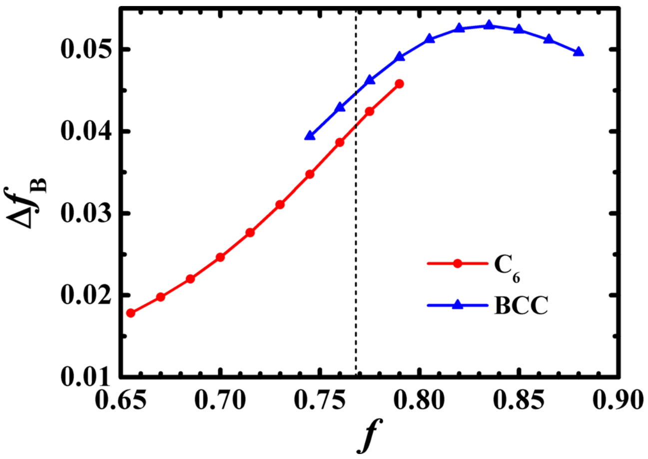

Figure 8. Deviation of the volume fraction of B-domains f_B^{eff} from the intrinsic volume fraction of B-blocks f_B, $\Delta f_B = f_B - f_B^{eff}$, as a function of f for $\tau = 1/3$ and $\chi N = 50$.

In contrast to the large region of the BCC phase in Figure 2b, a considerable region of the σ phase as well as a noticeable window of the A15 phase is observed in the expanded overall spherical region in the phase diagram of Figure 2d. Our SCFT calculations reveal that the spherical domains in the Frank−Kasper σ or A15 phase are enlarged in accord with the volume fraction of B-blocks. Furthermore, the separate density distributions of B_1- and B_2-blocks indicate that the enlarged B-domains are "core−shell" structure where the "core" is mainly composed of the long B_1-blocks while the "shell" is formed by the short jointed B_2-blocks (Figure 9). In other words, the large B-domains are formed via the local intramolecular segregation between the two different B-blocks along the radial direction of the domain, thus stabilizing the complex Frank−Kasper phases. In our previous work, the inter/intramolecular segregation between different polymers/blocks as an important sophisticated mechanism has been successfully applied to stabilize various unconventional ordered phases including the Frank−Kasper spherical phases,[52,73] the Laves phases,[32] the PL phase,[23] and the hybrid phases.[19]

Another remarkable phase behavior lies in the absence of the gyroid phase with A-network (G_A) in the phase diagram of Figure 2d, which is in obvious contrast to the general phase sequence of BCC → C_6 → G → L observed in the self-assembly of many AB-type block copolymers.[15] The typical comparison of free energies in Figure 10 indicates that the G_A

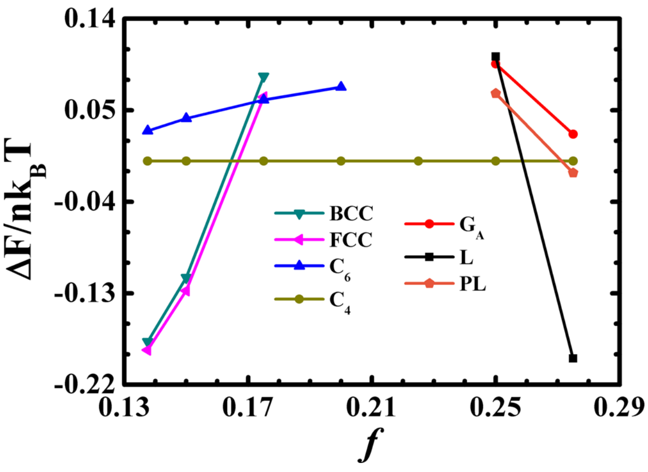

Figure 10. Free energies of considered ordered phases relative to that of the C_4 phase along the phase path of $\chi N = 50$ in the phase diagram of Figure 2d with $\tau = 4/5$, indicating the absence of the G_A phase.

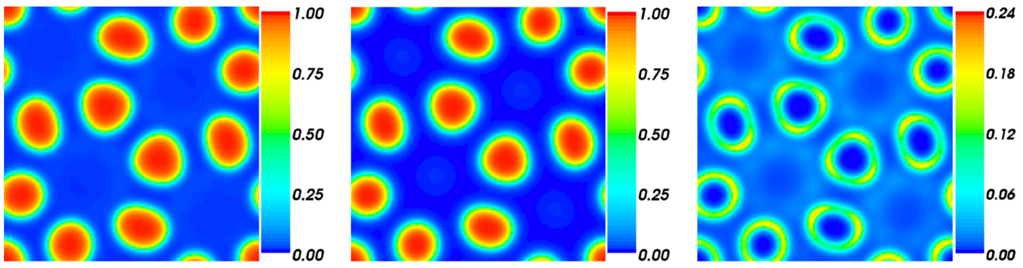

Figure 9. Typical density plots of the σ phase indicating the core−shell structure of domains for $\chi N = 50$, $f = 0.775$, and $\tau = 0.8$. The left panel shows the total volume fraction of B-blocks, while the middle and right panels show the volume fractions of B_1-block and B_2-block, respectively.

DOI: 10.1021/acs.macromol.8b01484
Macromolecules 2018, 51, 9890−9900

phase has considerably higher free energy than the corresponding C_4 or L phase or even higher than the PL phase. Similar results have been reported in the previous study of the $(ABA)_3$-triblock star copolymers by Fredrickson's group.[55] They observed that the phase region of G_B is vanishingly narrow at $\tau \approx 0.93$ in the f_A−τ phase diagram of the $(ABA)_3$ star copolymers. We speculate that the complete vanishing of the G_A phase in the phase diagram of $\tau = 4/5$ should be resulted in by the highly stretched bridging B_2-blocks which originates from the effect of combinatorial entropy of the multiple arms. In the morphologies of discrete domains, the high stretching could be further released by lowering the coordination number of the crystallline lattice of the discrete domains, such as changing C_6 to C_4. However, this kind of transition cannot occur in the fixed coordinate environment of G_A, which makes the G_A phase be less favorable.

In addition to the unusual phase behaviors discussed above, the change of the phase region of O^{70} as τ varies is also very interesting. For example, in the side of the phase diagram of Figure 2b where A is the minority component, the phase region of O^{70} is significantly enlarged, especially largely extended toward the strong segregation region. Such a large region of O^{70} facilitates its observation in experiments. In fact, this phenomenon has also been observed in other highly asymmetric phase diagrams of AB-type block copolymers, such as in the phase diagrams of AB_n miktoarm star copolymers.[15] More surprisingly, no stability region of O^{70} is predicted in either side of the phase diagrams of Figure 2c,d. In particular, the absence of O^{70} in either side of the highly asymmetric phase diagram of Figure 2d is very unusual and is in great contrast to the enlarged region of O^{70} in Figure 2b. The typical free energy comparison for $\chi N = 18$ is presented in Figure 11. However, we do not have an explanation for the unusual phase behavior of the O^{70} phase.

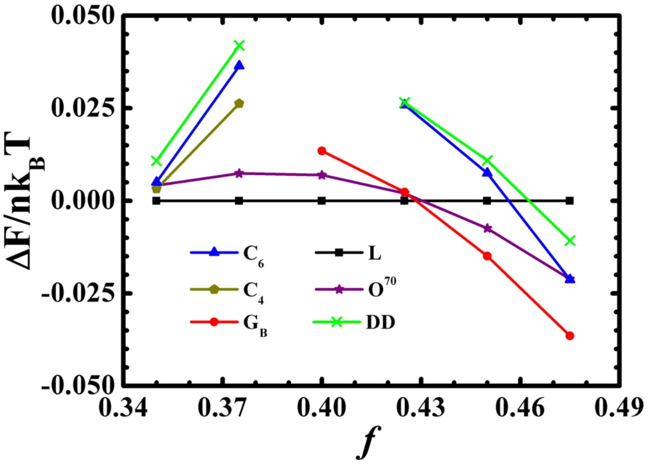

Figure 11. Free energies of considered ordered phases relative to that of the L phase along the phase path of $\chi N = 18$ in the phase diagram of Figure 2d with $\tau = 4/5$, indicating the absence of the O^{70} phase.

To obtain more direct understanding on the influence of τ on the phase behavior of the $(B_1AB_2)_5$ star copolymers, we construct the phase diagram at the f−τ plane for fixed $\chi N = 50$ in Figure 12. This phase diagram is similar to but also noticeably different from that of $(ABA)_3$.[55] On the one hand, those unusual phase behaviors summarized from Figure 2 are more clearly exhibited, such as the reentrant BCC/FCC transitions indicated by the presence of two FCC regions and the disappearance of the G_A phase indicated by the C_4/L phase boundary. On the other hand, more interesting ordered phases are predicted, i.e., the sandwich-like lamellar (L′) and hybrid lamella−sphere (LS) morphologies. The formation mechanism of the two ordered phases is similar to that in our previous ABAB tetrablock copolymers.[19]

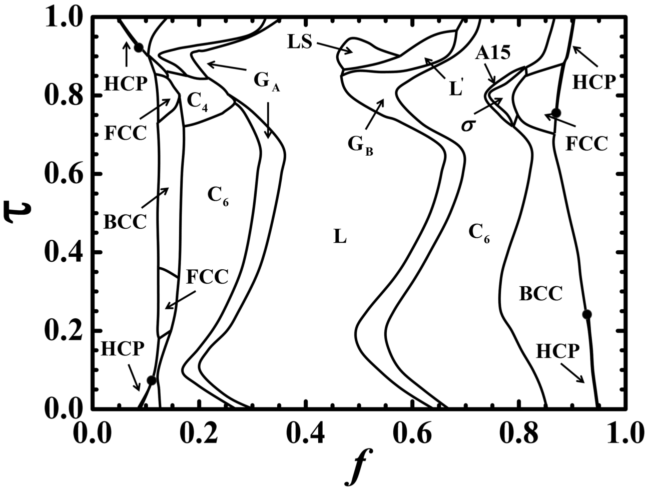

Figure 12. Phase diagram at the f−τ plane of $(B_1AB_2)_5$ star copolymers with $\chi N = 50$.

■ CONCLUSIONS

In summary, the phase diagrams of $(B_1AB_2)_5$ star copolymers at the f−χN plane for various values of $\tau = f_{B_1}/f_B$ have been constructed using the self-consistent field theory. Many unusual self-assembly behaviors have been observed in these phase diagrams with $0 < \tau < 1$, suggesting that τ is an important control parameter for the phase behavior of $(B_1AB_2)_5$ star copolymers. These unusual phase behaviors occur with different ordered phases including the spherical, cylindrical, and network (G and O^{70}) phases. For the spherical phases, interesting features are observed with either A-minority or B-minority side of the phase diagram. At the A-minority side, interesting reentrant BCC/FCC transitions, i.e., BCC → FCC→ BCC → FCC → BCC, are observed as τ increases. While at the opposite side, the overall phase region of spheres experiences a very surprising change, i.e., that those at $\tau = 1/3$ and at $\tau = 4/5$ are considerably wider than those at $\tau = 0$ and $\tau = 2/3$. The overall spherical region at $\tau = 1/3$ is expanded by the reduced effective volume fraction of B-blocks due to the solubilization of the short tail B_1-blocks into A-matrix, and thus the spherical domain is not significantly enlarged. In contrast, the expansion of the spherical region at $\tau = 4/5$ originates from the local segregation between the core B_2-blocks and the tail B_1-blocks along the radial direction of each domain, leading to the enlarged core−shell domains. As a consequence, the Frank−Kasper phases become stable in the side of the phase diagram for $\tau = 4/5$ where B is the minority component.

Another very surprising result lies in the absence of the gyroid phase composed of A-network (e.g., G_A) in the phase diagram of $\tau = 4/5$, which is rarely observed with the phase diagrams of AB-type block copolymers. It is also interesting to note that the phase region of G_B is largely expanded, thus facilitating its fabrication in experiments. It is speculated that

DOI: 10.1021/acs.macromol.8b01484
Macromolecules 2018, 51, 9890−9900

this unusual behavior may be induced by the highly stretched bridging B_2-blocks. In addition, unusual behaviors are also observed with the O^{70} phase,[37] i.e., exhibiting highly expanded region with A-minority in the phase diagram at $\tau = 1/3$ or even no stability region in the whole phase diagrams at $\tau = 2/3$ and $\tau = 4/5$. In brief, the self-assembly of $(B_1AB_2)_n$ star copolymers with tunable parameter $\tau = f_{B_1}/f_B$ exhibits many remarkable unusual behaviors and thus may be worth being studied by further experiments. Consider that the star copolymer is not difficult to be synthesized, our phase diagrams would provide useful guides for experiments to verify these unusual phase behaviors.

AUTHOR INFORMATION

Corresponding Author

*E-mail: weihuali@fudan.edu.cn.

ORCID

Weihua Li: 0000-0002-5133-0267

Notes

The authors declare no competing financial interest.

ACKNOWLEDGMENTS

This work was supported by National Natural Science Foundation of China (Grants 21774025 and 21574026).

REFERENCES

(1) Bates, F. S.; Fredrickson, G. H. Block Copolymer Thermodynamics:Theory and Experiment. *Annu. Rev. Phys. Chem.* **1990**, *41*, 525−557.

(2) Park, M.; Harrison, C.; Chaikin, P. M.; Register, R. A.; Adamson, D. H. Block Copolymer Lithography: Periodic Arrays of 10^{11} Holes in 1 Square Centimeter. *Science* **1997**, *276*, 1401−1404.

(3) Darling, S. B. Directing the Self-Assembly of Block Copolymers. *Prog. Polym. Sci.* **2007**, *32*, 1152−1204.

(4) Hong, A. J.; Liu, C. C.; Wang, Y.; Kim, J. Y.; Xiu, F. X.; Ji, S. X.; Zou, J.; Nealey, P. F.; Wang, K. L. Metal Nanodot Memory by Self-Assembled Block Copolymer Lift-Off. *Nano Lett.* **2010**, *10*, 224−229.

(5) Ji, S. X.; Nagpal, U.; Liao, W.; Liu, C. C.; de Pablo, J. J.; Nealey, P. F. Three-Dimensional Directed Assembly of Block Copolymers Together with Two-Dimensional Square and Rectangular Nanolithography. *Adv. Mater.* **2011**, *23*, 3692−3697.

(6) Pang, X. C.; Zhao, L.; Han, W.; Xin, X. K.; Lin, Z. A General and Robust Strategy for the Synthesis of Nearly Monodisperse Colloidal Nanocrystals. *Nat. Nanotechnol.* **2013**, *8*, 426−431.

(7) Li, W. H.; Müller, M. Defects in the Self-Assembly of Block Copolymers and Their Relavance for Directed Self-Assembly. *Annu. Rev. Chem. Biomol. Eng.* **2015**, *6*, 187−216.

(8) Ji, S. X.; Wan, L.; Liu, C. C.; Nealey, P. F. Directed Self-Assembly of Block Copolymers on Chemical Patterns: A Platform for Nanofabrication. *Prog. Polym. Sci.* **2016**, *54−55*, 76−127.

(9) Cao, X.; Mao, W. T.; Mai, Y. Y.; Han, L.; Che, S. A. Formation of Diverse Ordered Structures in ABC Triblock Terpolymer Templated Macroporous Silicas. *Macromolecules* **2018**, *51*, 4381−4396.

(10) Bates, F. S.; Hillmyer, M. A.; Lodge, T. P.; Bates, C. M.; Delaney, K. T.; Fredrickson, G. H. Multiblock Polymers: Panacea or Pandora's Box? *Science* **2012**, *336*, 434−440.

(11) Matsen, M. W. The Standard Gausian Model for Block Copolymer Melts. *J. Phys.: Condens. Matter* **2002**, *14*, R21−R47.

(12) Shi, A.-C. *Developments in Block Copolymer Science and Technology*; John Wiley & Sons, Ltd.: New York, 2004.

(13) Fredrickson, G. H. *The Equilibrium Theory of Inhomogeneous Polymers*; Oxford University Press: New York, 2006.

(14) Tyler, C. A.; Morse, D. C. Orthorhombic Fddd Network in Triblock and Diblock Copolymer Melts. *Phys. Rev. Lett.* **2005**, *94*, 208302.

(15) Matsen, M. W. Effect of Architecture on the Phase Behavior of AB-Type Block Copolymer Melts. *Macromolecules* **2012**, *45*, 2161−2165.

(16) Xie, N.; Liu, M. J.; Deng, H. L.; Li, W. H.; Qiu, F.; Shi, A.-C. Macromolecular Metallurgy of Binary Mesocrystals via Designed Multiblock Terpolymers. *J. Am. Chem. Soc.* **2014**, *136*, 2974−2977.

(17) Gao, Y.; Deng, H. L.; Li, W. H.; Qiu, F.; Shi, A.-C. Formation of Nonclassical Ordered Phases of AB-Type Multiarm Block Copolymers. *Phys. Rev. Lett.* **2016**, *116*, 068304.

(18) Arora, A.; Qin, J.; Morse, D. C.; Delaney, K. T.; Fredrickson, G. H.; Bates, F. S.; Dorfman, K. D. Broadly Accessible Self-Consistent Field Theory for Block Polymer Materials Discovery. *Macromolecules* **2016**, *49*, 4675−4690.

(19) Zhao, B.; Jiang, W. B.; Chen, L.; Li, W. H.; Qiu, F.; Shi, A.-C. Emergence and Stability of a Hybrid Lamella-Sphere Structure from Linear ABAB Tetrablock Copolymers. *ACS Macro Lett.* **2018**, *7*, 95−99.

(20) Matsen, M. W.; Thompson, R. B. Equilibrium Behavior of Symmetric ABA Triblock Copolymer Melts. *J. Chem. Phys.* **1999**, *111*, 7139−7146.

(21) Xie, N.; Li, W. H.; Qiu, F.; Shi, A.-C. σ Phase Formed in Conformationally Asymmetric AB-Type Block Copolymers. *ACS Macro Lett.* **2014**, *3*, 906−910.

(22) Spencer, R. K. W.; Matsen, M. W. Domain Bridging in Thermoplastic Elastomers of Star Block Copolymer. *Macromolecules* **2017**, *50*, 1681−1687.

(23) Jiang, W. B.; Qiang, Y. C.; Li, W. H.; Qiu, F.; Shi, A.-C. Effects of Chain Topology on the Self-Assembly of AB-Type Block Copolymers. *Macromolecules* **2018**, *51*, 1529−1538.

(24) Mai, S.-M.; Mingvanish, W.; Turner, S. C.; Chaibundit, C.; Fairclough, J. P. A.; Heatley, F.; Matsen, M. W.; Ryan, A. J.; Booth, C. Microphase-Separation Behavior of Triblock Copolymer Melts. Comparison with Diblock Copolymer Melts. *Macromolecules* **2000**, *33*, 5124−5130.

(25) Lee, S.; Bluemle, M. J.; Bates, F. S. Discovery of a Frank-Kasper σ Phase in Sphere-Forming Block Copolymer Melts. *Science* **2010**, *330*, 349−353.

(26) Lee, S. W.; Leighton, C.; Bates, F. S. Sphericity and Symmetry Breaking in the Formation of Frank-Kasper Phases from One Component Materials. *Proc. Natl. Acad. Sci. U. S. A.* **2014**, *111*, 17723−17731.

(27) Shi, W. C.; Lynd, N. A.; Montarnal, D.; Luo, Y. D.; Fredrickson, G. H.; Kramer, E. J.; et al. Toward Strong Thermoplastic Elastomers with Asymmetric Miktoarm Block Copolymer Architectures. *Macromolecules* **2014**, *47*, 2037−2043.

(28) Shi, W. C.; Tateishi, Y. C.; Li, W.; Hawker, C. J.; Fredrickson, G. H.; Kramer, E. J. Producing Small Domain Features Using Miktoarm Block Copolymers with Large Interaction Parameters. *ACS Macro Lett.* **2015**, *4*, 1287−1292.

(29) Chen, Y. H.; Yoon, Y. J.; Pang, X. C.; He, Y. J.; Jung, J. H.; Feng, C. W.; Zhang, G. Z.; Lin, Z. Q. Precisely Size-Tunable Monodisperse Hairy Plasmonic Nanoparticles via Amphiphilic Star-Like Block Copolymers. *Small* **2016**, *12*, 6714−6723.

(30) Li, W. H.; Duan, C.; Shi, A.-C. Non-Classical Spherical Packing Phases Self-Assembled From AB-Type Block Copolymers. *ACS Macro Lett.* **2017**, *6*, 1257−1262.

(31) Kim, K.; Schulze, M. W.; Arora, A.; Lewis, R. M.; Hillmyer, M. A.; Dorfman, K. D.; Bates, F. S. Thermal Processing of Diblock Copolymer Melts Mimics Metallurgy. *Science* **2017**, *356*, 520−523.

(32) Kim, K.; Arora, A.; Lewis, R. M.; Liu, M. J.; Li, W. H.; Shi, A. C.; Dorfman, K. D.; Bates, F. S. Origins of Low-Symmetry Phases in Asymmetric Diblock Copolymer Melts. *Proc. Natl. Acad. Sci. U. S. A.* **2018**, *115*, 847−854.

(33) Zhang, L. S.; Lin, J. P.; Lin, S. L. Effect of Molecular Architecture on Phase Behavior of Graft Copolymers. *J. Phys. Chem. B* **2008**, *112*, 9720−9728.

(34) Matsen, M. W.; Schick, M. Stable and Unstable Phases of a Diblock Copolymer Melt. *Phys. Rev. Lett.* **1994**, *72*, 2660−2663.

(35) Hajduk, D. A.; Harper, P. E.; Gruner, S. M.; Honeker, C. C.; Kim, G.; Thomas, E. L.; Fetters, L. J. The Gyroid: A New Equilibrium Morphology in Weakly Segregated Diblock Copolymers. *Macromolecules* **1994**, *27*, 4063−4075.

(36) Matsen, M. W. Equilibrium Behavior of Asymmetric ABA Triblock Copolymer Melts. *J. Chem. Phys.* **2000**, *113*, 5539−5544.

(37) Li, W.; Delaney, K. T.; Fredrickson, G. H. Fddd Network Phase in ABA Triblock Copolymer Melts. *J. Polym. Sci., Part B: Polym. Phys.* **2016**, *54*, 1112−1117.

(38) Sakurai, S.; Shirouchi, K.; Munakata, S.; Kurimura, H.; Suzuki, S.; Watanabe, J.; Oda, T.; Shimizu, N.; Tanida, K.; Yamamoto, K. Morphology Reentry with a Change in Degree of Chain Asymmetry in Neat Asymmetric Linear A_1BA_2 Triblock Copolymers. *Macromolecules* **2017**, *50*, 8647−8657.

(39) Matsen, M. W.; Schick, M. Stable and Unstable Phases of a Linear Multiblock Copolymer Melt. *Macromolecules* **1994**, *27*, 7157−7163.

(40) Spontak, R. J.; Smith, S. D. Perfectly-Alternating Linear $(AB)_n$ Multiblock Copolymers: Effect of Molecular Design on Morphology and Properties. *J. Polym. Sci., Part B: Polym. Phys.* **2001**, *39*, 947−955.

(41) Nagata, Y.; Masuda, J.; Noro, A.; Cho, D.; Takano, A.; Matsushita, Y. Preparation and Characterization of a Styrene-Isoprene Undecablock Copolymer and Its Hierarchical Microdomain Structure in Bulk. *Macromolecules* **2005**, *38*, 10220−10225.

(42) Nap, R.; Sushko, N.; Erukhimovich, I.; ten Brinke, G. Double Periodic Lamellar-in-Lamellar Structure in Multiblock Copolymer Melts with Competing Length Scales. *Macromolecules* **2006**, *39*, 6765−6770.

(43) Zhang, L. S.; Lin, J. P. Hierarchically Ordered Nanocomposites Self-Assembled from Linear-Alternating Block Copolymer/Nanoparticle Mixture. *Macromolecules* **2009**, *42*, 1410−1414.

(44) Ahn, S.; Kim, J. K.; Zhao, B.; Duan, C.; Li, W. H. Morphology Transitions of Linear $A_1B_1A_2B_2$Tetrablock Copolymers at Symmetric Overall Volume Fraction. *Macromolecules* **2018**, *51*, 4415−4421.

(45) Matsen, M. W.; Schick, M. Microphase Separation in Starblock Copolymer Melts. *Macromolecules* **1994**, *27*, 6761−6767.

(46) Xu, Y. C.; Li, W. H.; Qiu, F.; Lin, Z. Q. Self-Assembly of 21-Arm Star-Like Diblock Copolymer in Bulk and Under Cylindrical Confinement. *Nanoscale* **2014**, *6*, 6844−6852.

(47) Pang, X. C.; Zhao, L.; Akinc, M.; Kim, J. K.; Lin, Z. Q. Novel Amphiphilic Multi-Arm, Star-Like Block Copolymers as Unimolecular Micelles. *Macromolecules* **2011**, *44*, 3746−3752.

(48) Burns, A. B.; Register, R. A. Mechanical Properties of Star Block Polymer Thermoplastic Elastomers with Glassy and Crystalline End Blocks. *Macromolecules* **2016**, *49*, 9521−9530.

(49) Matsen, M. W.; Bates, F. S. Origins of Complex Self-Assembly in Block Copolymers. *Macromolecules* **1996**, *29*, 7641−7644.

(50) Li, W. H.; Shi, A.-C. *Self-Assemblying Systems Theory and Simulation*; John Wiley & Sons, Ltd.: New York, 2017; pp 85−107.

(51) Liu, M. J.; Xia, B. K.; Li, W. H.; Qiu, F.; Shi, A.-C. Self-Assembly of Binary Mesocrystals from Blends of BABCB Multiblock Copolymers and ABC Triblock Copolymers. *Macromolecules* **2015**, *48*, 3386−3394.

(52) Liu, M. J.; Qiang, Y. C.; Li, W. H.; Qiu, F.; Shi, A.-C. Stabilizing the Frank-Kasper Phases via Binary Blends of AB Diblock Copolymers. *ACS Macro Lett.* **2016**, *5*, 1167−1171.

(53) Beyer, F. L.; Gido, S. P.; Uhrig, D.; Mays, J. W.; Tan, N. B.; Trevino, S. F. Morphological Behavior of A 2B 2 Star Block Copolymers. *J. Polym. Sci., Part B: Polym. Phys.* **1999**, *37*, 3392−3400.

(54) Grason, G. M.; Kamien, R. D. Interfaces in Diblocks: A Study of Miktoarm Star Copolymers. *Macromolecules* **2004**, *37*, 7371−7380.

(55) Lynd, N. A.; Oyerokun, F. T.; O'Donoghue, D. L.; Handlin, D. L., Jr.; Fredrickson, G. H. Design of Soft and Strong Thermoplastic Elastomers Based on Nonlinear Block Copolymer Architectures Using Self-Consistent-Field Theory. *Macromolecules* **2010**, *43*, 3479−3486.

(56) Jiang, W. B.; Qiang, Y. C.; Liu, M. J.; Li, W. H.; Qiu, F.; Shi, A.-C. Tetragonal Phase of Cylinders Self-Assembled from Binary Blends of AB Diblock and $(A'B)_n$ Star Copolymers. *Phys. Chem. Chem. Phys.* **2017**, *19*, 25754−25763.

(57) Hayashida, K.; Dotera, T.; Takano, A.; Matsushita, Y. Polymeric Quasicrystal: Mesoscopic Quasicrystalline Tiling in ABC Star Polymers. *Phys. Rev. Lett.* **2007**, *98*, 195502.

(58) Matsushita, Y. Creation of Hierarchical Ordered Nanophase Structures in Block Polymers having Various Competing Interactions. *Macromolecules* **2007**, *40*, 771−776.

(59) Li, W. H.; Xu, Y. C.; Zhang, G. J.; Qiu, F.; Yang, Y. L.; Shi, A. C. Real-Space Self-Consistent Mean-Field Theory Study of ABC Star Triblock Copolymers. *J. Chem. Phys.* **2010**, *133*, 064904.

(60) Lee, W. B.; Elliott, R.; Mezzenga, R.; Fredrickson, G. H. Novel Phase Morphologies in a Microphase-Separated Dendritic Polymer Melt. *Macromolecules* **2009**, *42*, 849−859.

(61) Matsen, M. W.; Bates, F. S. Conformationally Asymmetric Block Copolymers. *J. Polym. Sci., Part B: Polym. Phys.* **1997**, *35*, 945−952.

(62) Kumar, R.; Fredrickson, G. H. Theory of Polyzwitterion Conformations. *J. Chem. Phys.* **2009**, *131*, 104901.

(63) Schulze, M. W.; Lewis, R. M.; Lettow, J. H.; Hickey, R. J.; Gillard, T. M.; Hillmyer, M. A.; Bates, F. S. Conformational Asymmetry and Quasicrystal Approximants in Linear Diblock Copolymers. *Phys. Rev. Lett.* **2017**, *118*, 207801.

(64) Shi, W. C.; Li, W.; Delaney, K. T.; Fredrickson, G. H.; Kramer, E. J.; Ntaras, C.; Avgeropoulos, A.; Lynd, N. A. Morphology Re-Entry in Asymmetric PS-PI-PS' Triblock Copolymer and PS Homopolymer Blends. *J. Polym. Sci., Part B: Polym. Phys.* **2016**, *54*, 169−179.

(65) Tzeremes, G.; Rasmussen, K. Ø.; Lookman, T.; Saxena, A. Efficient Computation of the Structural Phase Behavior of Block Copolymers. *Phys. Rev. E: Stat. Phys., Plasmas, Fluids, Relat. Interdiscip. Top.* **2002**, *65*, 041806.

(66) Rasmussen, K. Ø.; Kalosakas, G. Improved Numerical Algorithm for Exploring Block Copolymer Mesophases. *J. Polym. Sci., Part B: Polym. Phys.* **2002**, *40*, 1777−1783.

(67) Stasiak, P.; Matsen, M. W. Efficiency of Pseudo-Spectral Algorithms with Anderson Mixing for the SCFT of Periodic Block-Copolymer Phases. *Eur. Phys. J. E: Soft Matter Biol. Phys.* **2011**, *34*, 110.

(68) Thompson, R.; Rasmussen, K.; Lookman, T. Improved Convergence in Block Copolymer Self-Consistent Field Theory by Anderson Mixing. *J. Chem. Phys.* **2004**, *120*, 31−34.

(69) Matsen, M. W. Comment on "Stability of Ordered Phases in Weakly Segregated Diblock Copolymer Systems". *Phys. Rev. Lett.* **1998**, *80*, 201.

(70) Matsen, M. W. Fast and Accurate SCFT Calculations for Periodic Block-Copolymer Morphologies using the Spectral Method with Anderson Mixing. *Eur. Phys. J. E: Soft Matter Biol. Phys.* **2009**, *30*, 361−369.

(71) Milner, S. T. Chain Architecture and Asymmetry in Copolymer Microphases. *Macromolecules* **1994**, *27*, 2333−2335.

(72) Matsen, M. W. Polydispersity-Induced Macrophase Separation in Diblock Copolymer Melts. *Phys. Rev. Lett.* **2007**, *99*, 148304.

(73) Liu, M. J.; Li, W. H.; Qiu, F.; Shi, A.-C. Stability of σ Phase in B_1AB_2C Tetrablock Terpolymers. *Soft Matter* **2016**, *12*, 6412−6421.